An Ultrasensitive Room-Temperature H2S Gas Sensor Based on 3D Assembly of Cu2O Decorated WS2 Nanomaterial

Aanchal Alagh*, Fatima Ezahra Annanouch*, Polona Umek, Carla Bittencourt, Jean Francois Colomer+, Eduard Llobet*

***Abstract*— In this work, we report on the fabrication of multilayered tungsten disulfide structures and demonstrate their remarkable gas sensing characteristics towards hydrogen sulfide gas. A continuous film of WS_2 was deposited by adopting a facile route combining aerosol-assisted chemical vapor deposition with H_2 free atmospheric pressure CVD technique. SEM, XRD, HRTEM, and Raman spectroscopy were used to investigate the morphology and composition of the grown material. The performance of WS_2 sensors in the detection of hydrogen sulfide has been studied and results indicate that the synthesized material behaves as a p-type semiconductor with high sensitivity towards H_2S at sub-ppm level. Moreover, results obtained from humidity cross-sensitivity of the sensor indicate that the fabricated WS_2 sensor remains functional for H_2S gas detection at ppm level (with a moderate decrease in response) when ambient humidity is increased to 50%. Regarding long term stability, the sensor shows a very stable response towards H_2S gas detection over a period of 10 months.**

***Index Terms*—2D, APCVD, gas sensor, H_2S, TMDs, WS_2**

I. INTRODUCTION

Hydrogen sulfide (H_2S) appears as a colourless gas having pungent odour of rotten eggs [1]. It is a highly toxic and flammable gas, which is commonly referred to as hydrosulfuric acid and is known by several other names such as sewer gas, stink damp, hepatic gas or manure gas [2]. This noxious gas occurs naturally in crude petroleum, natural gas, volcanoes and hot springs[3][4]. Moreover, it is produced as a by-product from industrial activities, including petroleum refining, food processing, water treatment, tanneries, paper mills and mining [5][4]. Additionally, it is naturally produced by bacterial breakdown of organic matter including human and animal wastes in the absence of oxygen, such as in sewers and swamps. Depending on the concentration present it has a characteristic odour, for instance at concentrations of as low as 5 ppm it has an odour of rotten eggs, whereas at higher concentrations above 100 ppm it deadens the sense of smell, which makes it a silent threat for potential victims [6]. The effect on health of such a poisonous gas depends on its concentration and duration of exposure. It has been reported that at lower concentrations it causes eye irritation with blurred vision and can also lead to unconsciousness via inhalation, whereas at higher concentrations it can occasionally lead to corneal ulceration resulting in permanently impaired vision. Moreover, at concentrations above 100 ppm, the gas acts upon the human nervous system, which leads to paralysis and, with prolonged exposure, it could even cause immediate death. Aside from the harmful health effects to humans, wet hydrogen sulphide can even corrode carbon steel and other metallic surfaces bringing out economic losses. Therefore the acceptable concentration of H_2S (recommended by the Scientific Advisory Board on Toxic Air Pollutants, USA) is set in the range of 20–100 ppb [7].

For this reason, it is necessary to constantly screen H_2S gas levels to forestall spills and limit work related dangers. In this regard semiconducting metal oxide based gas sensors have been extensively studied for real-time monitoring of numerous hazardous gases at ppb levels as they offer multiple advantages over other sensing materials investigated [4]. The major advantages of these metal-oxide chemoresistive sensors are their small size, easy fabrication, low weight, and low cost [8]. Therefore, several metal oxide semiconductors have been investigated as active sensing material for H_2S gas detection. For instance, SnO_2 thin films have shown promising results in detecting H_2S gas in the range 1-15 ppm at room temperature, where the gas sensing properties were enhanced when SnO_2 films were modified with CuO resulting in faster response (20 s) and recovery times (40 s) [9]. Also, ZnO strikes as a most appealing sensing material showing superior detectability with detection limit as low as 20 ppb for H_2S gas [10]. In another work, similar detectability of 20 ppb has been achieved using WO_3 nanoparticle films [11]. However, limited selectivity against other interfering gases and high working temperature have hindered the practical applications of metal oxide based sensors for H_2S gas detection. In addition, metal oxide sensors often show poor long-term stability when exposed to H_2S as the corrosive nature of this gas alters both their microstructure and chemical composition [4].

Accordingly, in line of improving the existing sensing performance of chemiresistive gas sensors, graphene, carbon nanotubes, phosphorene and 2D transition metal dichalcogenide have attracted much attention to replace metal oxides [12][13][14]. The use of graphene as the active sensing material has been widely explored owing to its remarkable properties of high thermal conductivity, large surface area, high carrier mobility and high Young's modulus. However, despite its outstanding properties, being a zero-bandgap material, it limits its applications in electronics. Complementary to graphene, 2D TMDs with their tunable band gap properties offer plentiful application for future electronics [14][15]. In TMD materials, partially-filled d-orbitals are responsible for their metallic conductivities while fully filled d-orbitals are responsible for their semiconducting properties [16]. Moreover,

their layered structure, which can be easily exfoliated into individual layers, large specific surface area, low operating temperature, flexibility and compatibility with silicon technology provides them with numerous opportunities to integrate in gas sensing technology. In light of this, recently many reports have been presented, focusing mainly on gas sensing applications of MoS_2 and WS_2 [17][18][19][20]. Analogous to MoS_2, the layered structure of WS_2 contains one layer of W atoms sandwiched between two layers of S atoms [21]. WS_2 is believed to have superior gas sensing properties than MoS_2 as it shows higher electron mobility at room temperature (up to 234 cm^2/Vs) [22] and chemical robustness [23]. However, research on WS_2 nanomaterials for chemical gas sensing, particularly for H_2S gas is very scarce because of the greater difficulty in achieving controllable growth of WS_2, which is attributed to the much higher melting point of tungsten precursors compared to the molybdenum ones and the resulting higher growth temperatures needed [24].

In this respect, we report here H_2S gas-sensing performance of WS_2 nanosheets grown by combining the aerosol assisted chemical vapour deposition (AACVD) method with the H_2 free atmospheric pressure hot-wall CVD technique. It was inferred from our previous findings that the morphology of the starting material (WO_3) plays a key role in determining the ultimate structure of the WS_2 nanosheets. Henceforth in line with our previous research here we have employed WS_2 nanotriangle-nanoneedles (WS_2 NTs/NNs) as the sensing material for developing a chemiresistive H_2S gas sensor. The gas-sensing performance of this material towards hydrogen sulfide (H_2S) has been studied under both dry and humid atmospheres.The sensing performance of the fabricated WS_2 NTs/NNs sensor are superior to those reported in literature for H_2S gas [17][25][26][27]. Conclusively, a discussion on the H_2S sensing mechanism for the 3D assembly of WS_2 nanosheets is provided.

II. EXPERIMENTAL SECTION

A. *Material synthesis*:

WS_2 multilayered nanosheets were grown in two-steps following the procedure as reported in our previous work [25]. In brief in the first step, WO_3 nanoneedles (NNs) were grown directly on commercial alumina substrates, via aerosol-assisted chemical vapor deposition (AACVD) technique as shown in Fig.1(a). 50 mg of tungsten hexacarbonyl ($W(CO)_6$) (purity 97%) dissolved in a mixture of 15 mL acetone and 5 mL methanol were first sonicated and then kept in an ultrasonic humidifier to generate vapors from the dissolution. Nitrogen gas with a flow of 1L/min was used as a carrier to transport the aerosol inside the heated deposition chamber, which was kept at a temperature of 400 °C. The duration of the complete growth process was about 45 min. After deposition, the samples were annealed at 400 °C for 3 h under synthetic air in a carbolite CWF 1200 muffle furnace.

In the second step, WS_2 nanosheets were obtained via sulfurization of the as-grown WO_3 nanofilms using an atmospheric pressure CVD technique as shown in Fig.1(b). In a typical process, 0.44 g sulphur (S) powder (99.5%), purchased

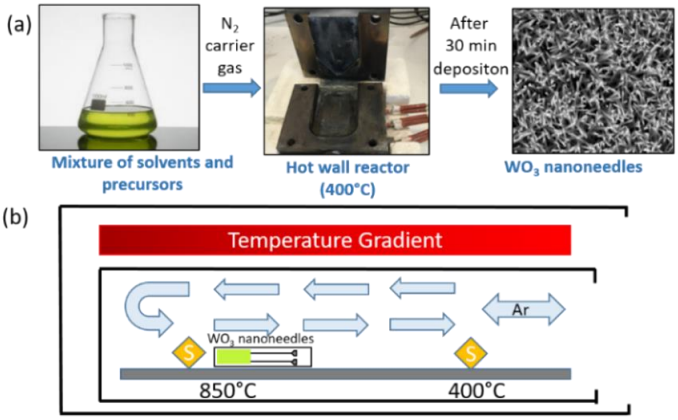

Fig. 1(a) WO_3 synthesis by AACVD process (b) WS_2 synthesis adopting CVD technique.

from Alfa Aesar was equally distributed in two ceramic boats and placed at different temperature zones of the furnace such that one was positioned at the 40 °C temperature zone and the other at 850 °C temperature zone. The substrate deposited with WO_3 nanomaterial in the first step was placed at the 850 °C temperature zone in the downstream of argon flow in the quartz tube reactor. Before the sulfurization process, the tube furnace was flushed with 0.725 L/min of argon gas to eliminate any oxygen content in the reactor. The primary step of sulfurization process goes for a period of 30 minutes (mins) during which the S powder set at the 850 °C zone sublimates. The second step of sulfurization was executed by pushing the quartz tube in the hot zone of the furnace, such that the S powder which was initially placed at 40 °C reaches the 400 °C temperature zone. As the quartz tube was pushed over a few centimeters, the WO_3 sample remained at 850 °C. After sulfurization, the furnace was naturally cooled down to room temperature.

B. *Sensor fabrication process and gas sensing measurement system*

For sensor processing, commercial alumina substrates which comprised interdigitated platinum electrodes with 300 µm electrode gap on the front side and a platinum (Pt) resistive heater meander on the backside were used. Fig.2 depicts an image of the commercial alumina substrate used. The gas sensing measurements were performed using a Teflon test chamber of 35 mL in volume, where up to four interdigitated alumina sensors can be placed and measured simultaneously. This chamber was connected to a fully automated, continuous gas flow measurement set-up able to supply diluted gas mixtures. The electrical resistance of sensors was measured using an Agilent-34972A multimeter.

Initially, the sensor was kept in a dry synthetic air flow (Air Premier Purity: 99.995%) at 100 mL/min for 4 h to stabilize its baseline resistance. The Pt heater meander was characterized to set the operating temperature of the sensor depending on the external power supply (Agilent, model 3492A). Dry air was chosen as the carrier and balance gas along all the experiments performed for the gas sensing characterization. Gas cylinders of H_2S (100 ppm in air) were used for the sensing measurements. The concentration of hydrogen sulfide gas was adjusted by controlling the flow rates of the target and balance gases with a

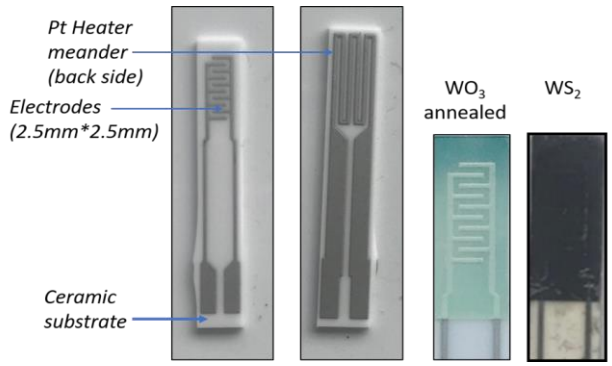

Fig. 2 Alumina transducer substrate used to deposit WO_3 nanomaterial (green color) and sulfurized to deposit WS_2 nanomaterial (black color).

total flow rate of 100 mL/min, which was kept constant throughout the measurements. After each sensing measurement the samples were cleaned in dry air for 1 h. Experiments under humid conditions were also conducted. For performing measurements in humid atmospheres, a computer-controlled humidification system was used, which comprises of a liquid mass flow and a mixer, to set the moisture level to 50% at 25 °C.

The gas sensing characteristics were examined in terms of response percentage, response time, recovery time, detection limit and repeatability. The sensor response is defined as percentile change in the baseline resistance of the sensor when exposed to an analyte gas. It can be calculated by using (1), given as:

$$\textbf{Response}\ (\%) = \left(\frac{\textbf{Rgas}-\textbf{Rair}}{\textbf{Rair}}\right) * \textbf{100} \qquad (1)$$

Here Rair and Rgas are respectively, the sensor resistance before and after exposure to H_2S gas. The response time is defined as the time required to reach 90% of the total resistance upon exposure to the target gas whereas the recovery time is defined as the time required to return to 90% of the original baseline resistance on removing the target gas [28].

C. Material Characterization

The crystalline structure of the as-grown WO_3 and WS_2 material was characterized using scanning electron microscope (SEM-FEI Quanta 600) whereas after the sulfurization process the morphology of the material was characterized using a field-emission scanning electron microscope Hitachi 2000 and FEI Helios Nanolab 650. A high-resolution transmission electron microscope (Jeol, JEM-2100) was used for crystallographic information at the atomic level. The images were acquired using a Gatan CCD camera ORIUS. For chemical phase analysis XRD measurements were made, using a Bruker-AXS D8-Discover diffractometer. Finally, Raman spectroscopy measurements were carried out using Renishaw in Via, laser 514 nm, ion argon-Novatech, 25 mW.

III. RESULTS AND DISCUSSION

A. Material synthesis and characterization

Scanning electron microscopy (SEM) gave an insight into the morphology and arrangement of the as-grown WO_3 and WS_2 nanomaterial. Fig.3(a) shows the SEM imaging results of the material prepared during the first step of synthesis.

In view of the results obtained, WO_3 grown by AACVD technique consisted of thin and elongated nanoneedles which were haphazardly aligned and evenly distributed on the alumina substrate. After sulfurization, the morphology of these nanoneedles changed completely to form a nanostructured film of WS_2 having a mixed morphology of nanotriangles (NTs) and nanoneedles (NNs), as shown in Fig.3(b) SEM image shows that WS_2 NTs are adhered to the WS_2 NNs and form an integral part of the nanostructured film in accordance with an arrangement that results a 3D architecture. The morphology and other characteristics of the grown WO_3 and WS_2 NTs/NNs hybrid material examined from SEM were identical to those reported in our previous work [29]. Additionally, it was deduced from our previous research work that the ultimate morphology of WS_2 nanofilms is dependent on the assembly of the starting material (WO_3) [29].

The as-grown WO_3 as well as WS_2 nanofilms were further investigated by using X-ray powder diffraction (XRD) to identify their crystallographic phase. Fig.4 displays the XRD pattern (upper spectrum) obtained for the grown WS_2 nanostructured film, which is compared with the spectrum of WO_3 NNs (lower spectrum) to detect the presence of any WO_3 impurities. From the diffractogram obtained, the diffraction peaks were perfectly indexed to the 2H-WS_2 [30]. The presence of sharp peaks in the spectrum further confirms the crystallinity of the grown nanofilms. Also, some peaks belonging to the alumina substrate were present [22] however peaks from any other impurity were not detected, indicating that a well-crystallized single phase WS_2 was obtained. Additionally, from the XPS analysis, no evidence on the presence of WO_3 impurities in the synthesized WS_2 films were detected [29]

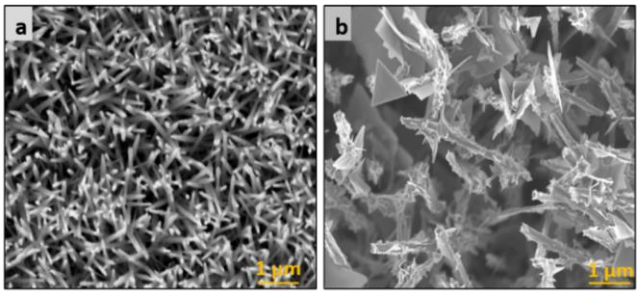

Fig. 3 SEM images of (a) WO_3 NNs, (b) nanostructured WS_2 film

Raman spectroscopy is a powerful technique to evaluate the crystal quality and film thickness of 2D materials and hence is used to analyze the as-synthesised material [31]. Fig.5 depicts Raman spectra obtained for the as-synthesised WO_3 and WS_2 nanofilms. The lower spectrum depicts peaks at 271 cm^{-1}, 327 cm^{-1}, 715 cm^{-1} and 805 cm^{-1}, which indicates the formation of monoclinic tungsten trioxide phase, which is in good accordance with our previous results [32]. From the upper

spectrum, the two main Raman active modes for 2H-WS_2 were found, E^1_{2g} at 348.5 cm^{-1} and A_{1g} at 414.5 cm^{-1}, where A_{1g} and E^1_{2g} mode indicates in plane and out-of-plane vibrations respectively. The sharp Raman peaks further indicates the crystallinity of the multilayered film, consistent with XRD results. Furthermore, it is possible to evaluate the number of layers present in the grown material by calculating the peak intensity difference between E^1_{2g} and A_{1g} mode (I E^1_{2g}/I A^{1g}). The observed difference of 0.89 indicates that the grown nanofilms consist of multilayers of WS_2, stacked together by van der Waals forces of interaction, which suppresses atom vibrations [33]. In addition, two broad peaks at 700 cm^{-1} and 803 cm^{-1}, were also detected with low intensity compared to WS_2 spectrum, indicating the presence of some WO_3 impurities.

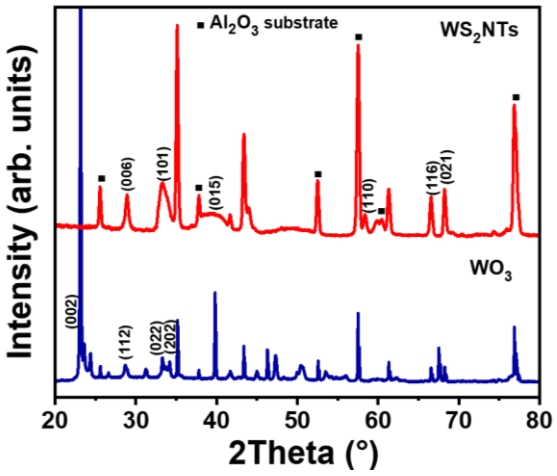

Fig. 4 XRD diffractograms for WO_3 NNs (bottom spectrum) and WS_2 NNs/NTs (upper spectrum)

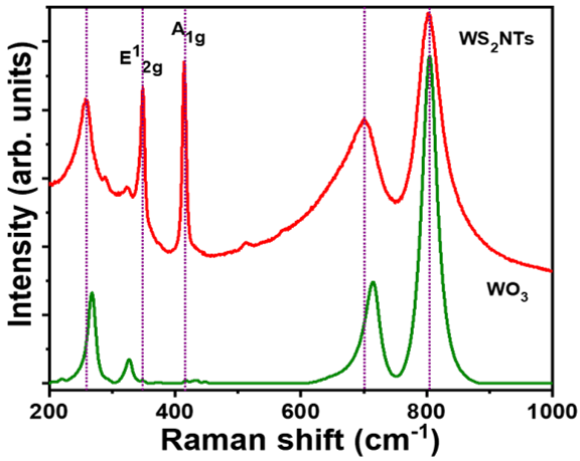

Fig. 5 Raman spectra of WO_3 NNs (lower spectrum), WS_2 NNs/ NTs (upper spectrum).

Hence it can be concluded that Raman spectroscopy is more sensitive than other characterization techniques at detecting traces of tungsten oxide which could be present within the bulk core of grown WS_2 films.

Observations from TEM and HRTEM are presented in Fig.6 wherein (a) shows characteristic WS_2 cluster composed of several 2D nanotriangles with side walls of about 800 nm. It appears that triangles are growing on top of one another. They are crystalline and no amorphous material is observed on their edges (Fig. 6b). Besides 2D nanostructures, also 1D nanostructures, i.e. nanoneedles, are observed. The characteristic interlayer distance of (002) planes in the nanoneedle close to the surface is 0.69 nm (Fig. 6c). The planes are expanded compared to the (002) planes in WS_2 single crystal most likely due to crystallographic defects, especially dislocations [34].

Thus, results from different characterization techniques performed, confirm the transformation of WO_3 nanomaterial to WS_2 with small traces of WO_3, which may be present in the bulk of the sulfurized multilayered nanofilms.

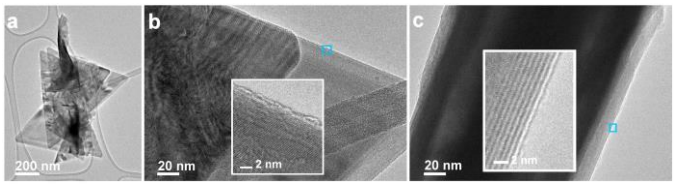

Fig. 6 TEM images of WS_2 cluster composed of nanotriangles with side wall of about 800 nm (a, b) and a middle part of the nanoneedle with diameter of 180 nm (c). Blue frames in images b and c indicate areas where HRTEM insets were taken.

B. Gas sensing Results and Discussion

In order to determine the gas sensing behavior of the fabricated WS_2 NTs/NNs sensor, it was exposed to a fixed concentration of H_2S gss (40 ppm) at three different temperatures, ranging from 25-150 °C. For all measurements, H_2S gas was injected for 10 mins followed by 50 mins purging with dry airflow so that the sensor can recover its initial baseline resistance. As plotted in Fig.7(a) the sensor response increases with increase in operating temperature, which clearly indicates more interactions between the target gas and the WS_2 sensing surface at higher temperature. One possible reason for this could be that higher temperature provides more energy to promote adsorption of H_2S gas molecules at the sensor surface, which results in higher response at an elevated temperature. However, measurements beyond 150 °C were not performed, since at temperatures above 150 °C sulfur could evaporate and could lead to the formation of a composite of tungsten oxide and sulfide. Thus, for subsequent studies, 150 °C was considered as the optimal working temperature for the fabricated WS_2 sensor. Consequently, lower operating temperature is one of the many advantages of using transition metal dichalcogenide based (such as WS_2 nanofilms) sensors for H_2S gas detection in comparison to the higher operating temperatures used for most metal oxide based H_2S gas sensors.

Furthermore, Fig.7(b) shows the dynamic electrical response for the fabricated WS_2 sensor towards 40 ppm of H_2S gas at 150 °C. The maximum gas response at 150 °C was 54.70 % for 40 ppm H_2S gas. To evaluate repeatability, the sensor was exposed to five sequences of the same concentrations of H_2S gas, the sensor showed high stability and good repeatability during the cyclic H_2S sensing tests. Moreover, it is observed that when the sensor is exposed to a reducing gas, the baseline resistance increases, indicating a p-type semiconducting behavior. This is

consistent to the results reported in the literature for WS_2 nanofilms [17][16][25][26][27].

The response time and recovery time were calculated to be 10.6 and 15.8 mins respectively when the sensor was exposed to 40 ppm of H_2S gas at 150 °C. To compare with previous works in literature [25], the fabricated WS_2 sensor takes comparatively longer time, which could possibly be associated with the greater difficulty in diffusion of H_2S moleules in the core of grown films. As a result the process of adsorption and desorption of gas molecules is extended for a longer duration. To improve the response/recovery time of WS_2 films, functionalization with metal nanoparticles could be done in future.

Furthermore, the sensor response drops down from 54.7% to 15.6% when the gas concentration is reduced from 40 ppm to 5 ppm . Nevertheless, a response value of 54.7% is significantly higher for WS_2 nanofilms that is ever reported in literature. Moreover, the sensor was also tested for H_2S 40 ppm at room temperature and surprisingly, the sensor showed an acceptable response of 10% with small drift which can be attributed to the slow desorption of gas molecules when operated at room temperature (Fig. S1).

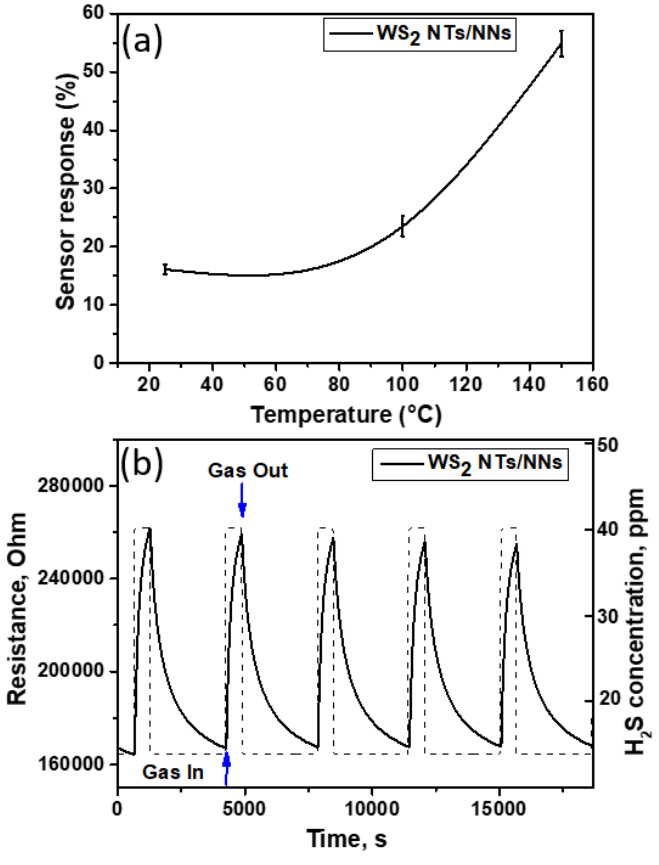

Fig. 7 WS_2 sensor response towards 40 ppm H_2S gas (a) as a function of temperature, (b) showing change in electrical resistance (5 replicate response and recovery cycles) when operated at 150 °C.

Fig.8, panel (a) shows the intensity of sensor responses as a function of H_2S gas concentration. It is observed that sensor response increased quite linearly with the increase in gas concentration (in the 5 to 40 ppm range). Also detection in the ppb range is validated from the results shown in Fig.8, panel (b) where the sensor is tested at three different concentrations of H_2S gas 300, 500 and 800 ppb at a constant operating temperature of 150 °C. Sensor responses were calculated to be 4.4%, 6.2% and 6.9% for 300, 500 and 800 ppb of hydrogen sulfide, respectively. Exposing the sensor to such low concentrations of H_2S gas revealed that the detection limit of this sensor for hydrogen sulfide is below 200 ppb (considering the intensity of the responses recorded and the noise level). Furthermore, Fig.9 panel (a) presents five replicate response and recovery cycles of a WS_2 sensor towards very low concentrations of H_2S gas (200 ppb). Evidently, the sensor displayed a response of 3.3% at such a low concentration with enough signal to noise ratio. Moreover, the sensor showed steady and reproducible responses which can be attributed to the direct growth of the sensing material on the sensor transducer which allows formation of perfect interfaces that would prevent degradation of the film.

Additionally, sensing characteristics of the fabricated WS_2 sensor for H_2S gas in humid environment were also tested and the corresponding results are shown in Fig.9 panel (b). The sensor was tested for 5 replicates towards 40 ppm of H_2S,

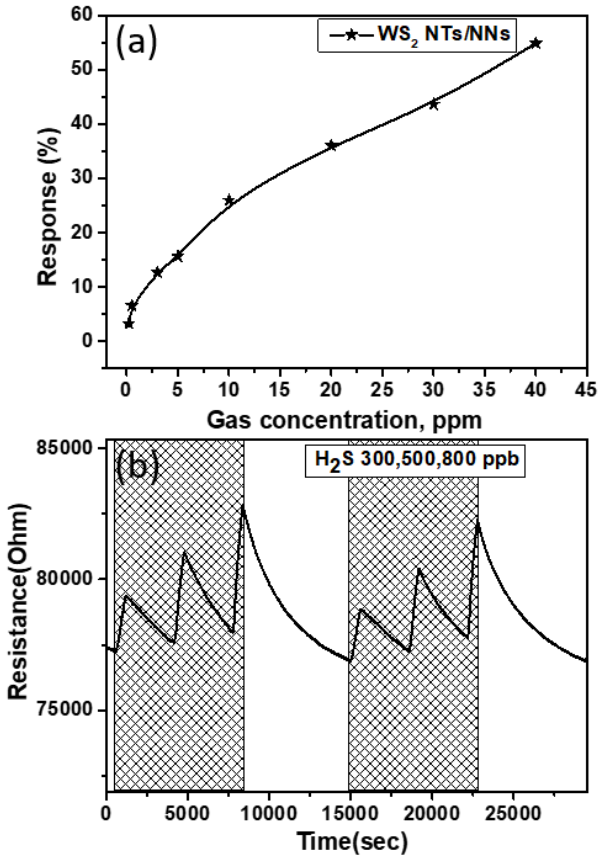

Fig. 8 WS_2 sensor response at 150 °C (a) as a function of different H_2S gas concentrations (0.2, 0.5, 3, 5, 10, 20, 30, 40 ppm), (b) showing change in electrical resistance for two replicate measurements for increasing concentration pulses (300, 500, 800 ppb).

operated at 150 °C in humid backgrounds with 50% RH. It was observed that the sensor response dropped down from 54.7% to

20% with the adsorption of water vapor on the WS_2 sensor surface which apart from changing the baseline resistance, blocks the reaction sites, also reported in literature [35].

Moreover, once the humidity measurements were done, the sensor was heated at a temperature of 100 °C under dry air flow for 48 hours to clean the sensor surface from water vapors and was tested again towards 40 ppm of H_2S at 150 °C. Surprisingly, it was observed that the sensor regained its initial sensitivity with sensing response of 52% and remained functional even after humidity exposure. It is very important to note here, that most of the reported studies on layered WS_2 gas sensors have not studied the effect of ambient humidity on sensing performance, which is an essential parameter for the practical application of gas sensors. In adittion to this, to verify the long term stability of the H_2S sensing properties we repeated the sensing tests after a period of 10 months from the first H_2S gas measurements and it was observed that there was no loss in the sensing ability of the sensor and the sensor displayed an excellent stability (Fig.S2).

In this respect, Table 1 gives more insights by comparing the performance in the detection of H_2S reported in this paper with those found in the literature. From the results obtained, it is clear that the fabricated WS_2 NTs/NNs sensor shows outstanding gas responses with high sensitivity towards H_2S gas and a detection limit below 200 ppb when operated at 150 °C. Besides that, the sensor remains functional and sensitive towards the targeted gas (H_2S) even at room temperature.

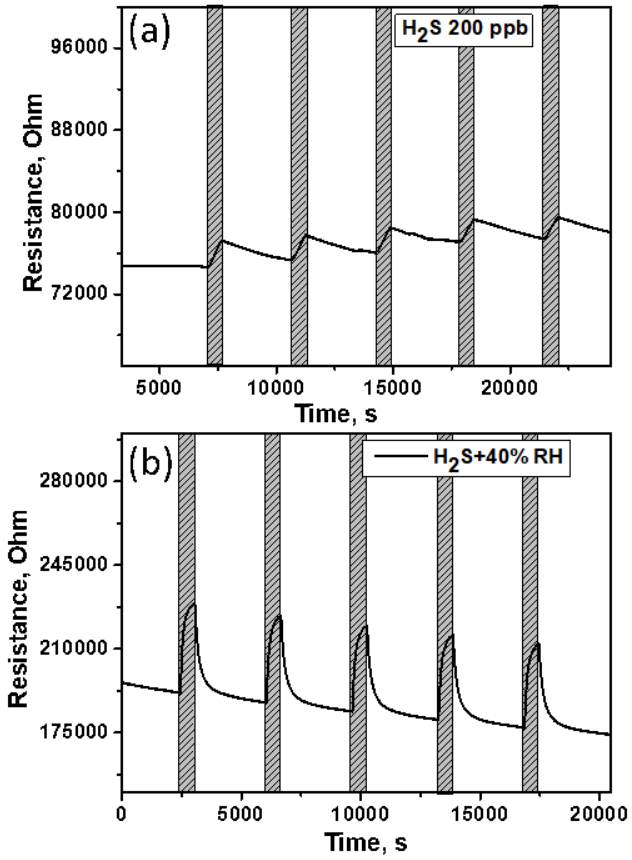

Fig. 9 (a) Electrical resistance of WS_2 sensor response at 150 °C towards (a) 200 ppb of H_2S, (b) 40 ppm H_2S gas in 50% RH background.

C. H_2S gas sensing mechanism

As demonstrated in gas sensing measurements, the WS_2 NTs/NNs based gas sensor revealed a p-type semiconducting behavior wherein the resistance increased in presence of H_2S gas. The sensing mechanism of WS_2 nanosheets is based on charge transfer process. When the sensor is exposed to a reducing gas such as H_2S in our case, the gas molecules get physiosorbed on the sensing layer resulting in change of electrical resistance of the material. H_2S being an electron donor donates electron which gets adsorbed by the multi-layered WS_2, thereby increasing the overall resistance of the material, which indicates p-type semiconducting behavior of the fabricated tungsten disulfide sensor. In this regard, many reports have revealed a similar behavior. According to previous research findings in literature, the adsorption energy for a monolayer WS_2 nanofilm for H_2S gas molecule is slightly lesser than that for bilayer WS_2 nanofilm which is –246.2 meV [25]. This suggests that as the number of layers increases from mono to multi layered WS_2, their corresponding adsorption energy towards H_2S increases resulting in a qualitatively higher sensitivity towards H_2S, which is in accordance with our experimental results for multilayered WS_2. The sensing performance of the present material, WS_2 nanotriangle and nanoneedle hybrids are however superior to those measured for WS_2 nanoflake-nanorod hybrid structure [25]. This can be attributed to the arrangement of nanotriangles and nanoneedles of tungsten disulphide such that there are more edges that are exposed to the gas molecules for adsorption. In addition to the high surface to volume ratio of nanoneedles, the nanotriangles offers more interspace, as a result, the assembly shows an increased porosity with a greater number of edges, resulting in availability of abundant active sites for gas interaction. Moreover, multilayered nanofilms offer more electron transfer channels for improved reaction between the material and target gas, in comparison to the more closely packed nanoflake assembly. This may explain the superior gas sensing properties recorded for WS_2 with nanotriangle and nanoneedle morphology.

Table 1. Comparison of the sensing properties of H_2S resistive and FET type gas sensors based on different WS_2 sensing material structures in the literature and WS_2 nanosheets in this study.

Material structure	Concentration (ppm)	Operating temp.(˚C)	Response (%)	Sensitivity (Response /ppm)	Detection limit	References
NTs/NNs	0.2	150	3.2	0.059	0.2 (exper)	This work
NTs/NNs	40	150	54.7	0.013	0.2 (exper)	This work
NTs/NNs	40	25	10.0	NA	N/A	This work
NS	5	160	14.0	N/A	N/A	[17]
NW-NF hybrid	1	200	N/A	0.023	0.02 (exper)	[25]
NW-NF hybrid	0.02	200	N/A	0.043	0.02 (exper)	[25]
NS 0	50	120	1.3 (Ra/Rg)	N/A	N/A	[26]
NP	10	100	7.2	0.007	N/A	[27]

N/A: Not available; experimentally measured; NTs/NNs; NTs/NNs: nanotriangles-nanoneedles; NS: nanosheets; NW-NF: nanowire-nanoflake; NP: nanoparticles

IV. CONCLUSION

We have investigated the H_2S gas sensing performance of WS_2 sensor fabricated directly on commercial sensor transducer via a simple CVD technique. The sensor is composed of a hybrid structure of nanoneedles and nanotriangles of WS_2 with high quality and crystallinity as confirmed by XRD, Raman and TEM characterization techniques. Our results demonstrate better sensing performance for WS_2 nanofilms with higher sensitivity towards H_2S than previously reported for WS_2 nanofilms. This is attributed to the porous surface and the increased number of sulfur edges in WS_2 NNs/NTs, which were created by the random 3D assembly of WS_2 nanotriangles on WS_2 nanoneedles. This leads us to conclude that the morphology and arrangement of WS_2 nanosheets plays a significant role for gas sensing. Hence our results could be beneficial for future H_2S gas sensing studies with commercial potential due to the stable and high responses attained at much lower operating temperatures (even room temperature) than those of metal oxides. Furthermore, the direct growth of WS_2 nanofilms on the sensor transducer with high degree of scalability and controllability makes the production of these nanofilms much more feasible.

Appendix

Supplementary material related to this article

ACKNOWLEDGMENTS

This project has received funding from the European Union's Horizon 2020 research and innovation programme under the Marie Skłodowska-Curie grant agreements No. 713679 and 823895 and from the Universitat Rovira i Virgili (URV). F.E.A. is a JdC fellow. E.L. is supported by the Catalan Agency for Research and Advanced Studies via the 2018 Edition of the ICREA Academia Award. CB and JFC are research associates of FNRS (Belgium).

REFERENCES

[1] J. Miao, C. Chen, and J. Y. S. Lin, "Humidity independent hydrogen sulfide sensing response achieved with monolayer film of CuO nanosheets," *Sensors Actuators, B Chem.*, vol. 309, p. 127785, 2020.

[2] H. Sulfide, "Hydrogen Sulfide (H 2 S)," *Heal. San Fr.*, vol. 19, no. 7, p. 2, 2005.

[3] S. K. Pandey, K. H. Kim, and K. T. Tang, "A review of sensor-based methods for monitoring hydrogen sulfide," *TrAC - Trends Anal. Chem.*, vol. 32, pp. 87–99, 2012.

[4] A. Mirzaei, S. S. Kim, and H. W. Kim, "Resistance-based H2S gas sensors using metal oxide nanostructures: A review of recent advances," *J. Hazard. Mater.*, vol. 357, pp. 314–331, 2018.

[5] C. H. Moon, M. Zhang, N. V. Myung, and E. D. Haberer, "Highly sensitive hydrogen sulfide (H2S) gas sensors from viral-templated nanocrystalline gold nanowires," *Nanotechnology*, vol. 25, no. 13, 2014.

[6] A. Mortezaali and R. Moradi, "The correlation between the substrate temperature and morphological ZnO nanostructures for H2S gas sensors," *Sensors Actuators, A Phys.*, vol. 206, pp. 30–34, 2014.

[7] Y. Guo, M. Gong, Y. Li, Y. Liu, and X. Dou, "Sensitive, Selective, and Fast Detection of ppb-Level H2S Gas Boosted by ZnO-CuO Mesocrystal," *Nanoscale Res. Lett.*, vol. 11, no. 1, 2016.

[8] T. Xu *et al.*, "The ultra-high NO2 response of ultra-thin WS2 nanosheets synthesized by hydrothermal and calcination processes," *Sensors Actuators, B Chem.*, vol. 259, no. 2, pp. 789–796, 2018.

[9] N. S. A. Eom, H. B. Cho, Y. Song, G. M. Go, J. Lee, and Y. H. Choa, "Room-temperature H2S gas sensing by selectively synthesized Cux(x=1,2)O:SnO2 thin film nanocomposites with oblique & vertically assembled SnO2 ceramic nanorods," *Sensors Actuators, B Chem.*, vol. 273, no. June, pp. 1054–1061, 2018.

[10] Z. S. Hosseini, A. I. Zad, and A. Mortezaali, "Room temperature H2S gas sensor based on rather aligned ZnO nanorods with flower-like structures," *Sensors Actuators, B Chem.*, vol. 207, no. PartA, pp. 865–871, 2015.

[11] W. Yu-De, C. Zhan-Xian, L. Yan-Feng, Z. Zhen-Lai, and W. Xing-Hui, "Electrical and gas-sensing properties of WO3 semiconductor material," *Solid. State. Electron.*, vol. 45, no. 5, pp. 639–644, 2001.

[12] C. Cong *et al.*, "Synthesis and optical properties of large-area single-crystalline 2D semiconductor WS2monolayer from chemical vapor deposition," *Adv. Opt. Mater.*, vol. 2, no. 2, pp. 131–136, 2014.

[13] J. Yu, J. Li, W. Zhang, and H. Chang, "Synthesis of high quality two-dimensional materials via chemical vapor deposition," *Chem. Sci.*, vol. 6, no. 12, pp. 6705–6716, 2015.

[14] W. Choi, N. Choudhary, G. H. Han, J. Park, D. Akinwande, and Y. H. Lee, "Recent development of two-dimensional transition metal dichalcogenides and their applications," *Mater. Today*, vol. 20, no. 3, pp. 116–130, 2017.

[15] T. Kim, Y. Kim, S. Park, S. Kim, and H. Jang, "Two-Dimensional Transition Metal Disulfides for Chemoresistive Gas Sensing: Perspective and Challenges," *Chemosensors*, vol. 5, no. 2, p. 15, 2017.

[16] E. Lee, Y. S. Yoon, and D. J. Kim, "Two-Dimensional Transition Metal Dichalcogenides and Metal Oxide Hybrids for Gas Sensing," *ACS Sensors*, vol. 3, no. 10, pp. 2045–2060, 2018.

[17] D. Liu, Z. Tang, and Z. Zhang, "Comparative study on NO2 and H2S sensing mechanisms of gas sensors based on WS2 nanosheets," *Sensors Actuators, B Chem.*, vol. 303, no. 2, p. 127114, 2020.

[18] V. Paolucci, S. M. Emamjomeh, M. Nardone, L. Ottaviano, and C. Cantalini, "Two-step exfoliation of WS2 for NO2, H2 and humidity sensing applications," *Nanomaterials*, vol. 9, no. 10, pp. 1–17, 2019.

[19] T. J rvinen *et al.*, "WS2 and MoS2 thin film gas sensors with high response to NH3 in air at low temperature," *Nanotechnology*, vol. 30, no. 40, 2019.

[20] J. Park, J. Mun, J. Shin, and S. Kang, "Highly sensitive two-dimensional MoS 2 gas sensor decorated with Pt nanoparticles," pp. 1–9, 2018.

[21] W. J. Schutte, J. L. D. E. Boer, and F. Jellinek, "Structures of Tungsten Disulfide and Diselenide "," vol. 209, pp. 207–209, 1987.

[22] P. Arod and S. A. Shivashankar, "Single-step synthesis of carbon nanotubes/iron/iron oxide composite films through inert-ambient

CVD using ferric acetylacetonate as a precursor," *RSC Adv.*, vol. 5, no. 73, pp. 59463–59471, 2015.

[23] V. A. Online, "hybrid structure for hydrogen evolution reaction †," pp. 4657–4661, 2013.

[24] B. Yorulmaz, A. Özden, H. Şar, F. Ay, C. Sevik, and N. K. Perkgöz, "CVD growth of monolayer WS 2 through controlled seed formation and vapor density," *Mater. Sci. Semicond. Process.*, vol. 93, no. January, pp. 158–163, 2019.

[25] G. A. Asres *et al.*, "Ultrasensitive H 2 S gas sensors based on p-type WS 2 hybrid materials," pp. 1–10, 2009.

[26] J. Kim, A. Mirzaei, H. Woo, and S. Sub, "Sensors and Actuators B : Chemical Realization of Au-decorated WS 2 nanosheets as low power-consumption and selective gas sensors," *Sensors Actuators B. Chem.*, vol. 296, no. February, p. 126659, 2019.

[27] Y. Jeong, J. Shin, Y. Hong, M. Wu, S. Hong, and K. Chang, "Gas sensing characteristics of the FET-type gas sensor having inkjet-printed WS 2 sensing layer," *Solid State Electron.*, vol. 153, no. December 2018, pp. 27–32, 2019.

[28] Z. U. Abideen, J. H. Kim, A. Mirzaei, H. W. Kim, and S. S. Kim, "Sensing behavior to ppm-level gases and synergistic sensing mechanism in metal-functionalized rGO-loaded ZnO nanofibers," *Sensors Actuators, B Chem.*, vol. 255, pp. 1884–1896, 2018.

[29] A. Alagh *et al.*, "CVD growth of self-assembled 2D and 1D WS2 nanomaterials for the ultrasensitive detection of NO2," *Sensors Actuators, B Chem.*, vol. 326, no. September 2020, p. 128813, 2021.

[30] T. A. J. Loh, D. H. C. Chua, and A. T. S. Wee, "One-step Synthesis of Few-layer WS2 by Pulsed Laser Deposition," *Sci. Rep.*, vol. 5, no. November, pp. 1–9, 2015.

[31] Y. Wu, Y. Hao, M. Fu, W. Jiang, and Q. Wu, "on domain structure and electrical performance," pp. 930–937, 2016.

[32] F. E. Annanouch *et al.*, "Aerosol-Assisted CVD-Grown WO 3 Nanoneedles Decorated with Copper Oxide Nanoparticles for the Selective and Humidity-Resilient Detection of H 2 S," 2015.

[33] F. Lan *et al.*, "Synthesis of Large-Scale Single-Crystalline Monolayer WS2 Using a Semi-Sealed Method," *Nanomaterials*, vol. 8, no. 2, p. 100, 2018.

[34] V. Weiß, S. Seeger, K. Ellmer, and R. Mientus, "Reactive magnetron sputtering of tungsten disulfide (W S2-x) films: Influence of deposition parameters on texture, microstructure, and stoichiometry," *J. Appl. Phys.*, vol. 101, no. 10, 2007.

[35] W. T. Koo *et al.*, "Few-Layered WS2 Nanoplates Confined in Co, N-Doped Hollow Carbon Nanocages: Abundant WS2 Edges for Highly Sensitive Gas Sensors," *Adv. Funct. Mater.*, vol. 28, no. 36, pp. 1–11, 2018.